Electrical Power and Energy Systems 104 (2019) 716–723

Contents lists available at ScienceDirect

Electrical Power and Energy Systems

journal homepage: www.elsevier.com/locate/ijepes

Metrics and quantitative framework for assessing microgrid resilience against windstorms

M.H. Amirioun[a], F. Aminifar[a,*], H. Lesani[a], M. Shahidehpour[b]

[a] School of Electrical and Computer Engineering, College of Engineering, University of Tehran, Tehran 11365-4563, Iran
[b] Electrical and Computer Engineering Department, Illinois Institute of Technology, Chicago, IL 60616, USA

ARTICLE INFO

Keywords:
Microgrids
Resilience
Fragility curves
High-impact low-probability events
Measure of performance (MoP)
Distributed energy resources (DERs)
Windstorm

ABSTRACT

Recent extreme weather events have emphasized the need for new methods and metrics to assess the power system resilience in response to high-impact low-probability (HILP) events. Microgrids (MGs) have been instrumental in such occasions for maintaining the power supply continuity to local customers. This paper provides a quantitative framework for assessing the MG resilience in response to HILP windstorms. The proposed framework jointly employs fragility curves of overhead distribution branches and windstorm profile to quantify the degradation in the MG performance (particularly supplied load in this work). The proposed analytical method is simple and computationally efficient which offers a quick means for getting knowledge about adverse impacts of an approaching windstorm and taking preventive measures accordingly. A set of normalized metrics is defined which provides a comparable tool for assessing the resilience in various operating conditions and power systems. The impacts of restorative actions, the system reinforcement, and the event severity on resilience curves and metrics are also investigated. The effectiveness of the proposed approach in response to an extreme windstorm is examined on a real-scale MG test bed.

1. Introduction

Power systems have conventionally been protected against low-impact high-probability events rendered by equipment breakdowns, human mistakes, or external interferences. The traditional protection schemes often ensured a reasonable level of reliability for power delivery to local customers [1,2]. The high-impact low-probability (HILP) events (i.e., extreme events) may also cause rare power outages with significantly greater damages in which socioeconomic impacts can extensively be stretched to larger and unpredictable parts of the power system [3]. Examples of these events include natural events such as hurricanes, typhoons, windstorms, blizzards, floods, earthquakes, as well as intentional cyber or physical attacks, and cascading failures [4–13]. The power system resilience is the ability of a power system to respond to HILP events and focuses on how rapidly and efficiently the power system can be restored to its pre-event operation state [3–5].

Appropriate metrics and modeling techniques are key elements in quantitative assessment of power system resilience. Unlike routine outages, HILP power outages may not be properly measured by reliability metrics which emphasize the duration and the frequency of power outages or the amount of energy not supplied. Although reliability indices can offer human operators with additional insight on the abnormal behavior of power systems, the static nature of these indices make them unsuitable for measuring the spatiotemporal impacts of HILP events on power grids [4]. New metrics are thus in essence for assessing the power system resilience.

Impacts of weather-originated HILP events on power systems are generally modeled by means of analytical and Monte Carlo (MC) simulation techniques. Analytical techniques are more applicable for small-scale power systems due to their simplicity and computational efficiency while simulation techniques are preferred for complex systems [14].

The literature on the power system resilience was reviewed in [15]. Refs. [14,16] made a comprehensive discussion on impacts of extreme events on the power system resilience. Authors in [14] presented a detailed discussion on modeling techniques for the assessment of adverse impacts on power systems incurred by weather-oriented HILP events. A few references in the literature presented conceptual (qualitative) frameworks for the power system resilience assessment using fragility curves of components [1,4,14,17]. Authors in [18] presented an uncertain risk assessment for catastrophic accidents based on a fuzzy approach. Ref. [19] employed a sequential MC-based time-series simulation method to quantify the adverse impacts of windstorms on power grid resilience. Reliability indices *LOLF* (loss of load frequency)

* Corresponding author.
E-mail addresses: mhamirioun@ut.ac.ir (M.H. Amirioun), faminifar@ut.ac.ir (F. Aminifar), lesani@ut.ac.ir (H. Lesani), ms@iit.edu (M. Shahidehpour).

https://doi.org/10.1016/j.ijepes.2018.07.025
Received 1 January 2018; Received in revised form 15 May 2018; Accepted 16 July 2018
Available online 02 August 2018

Nomenclature

Indices and sets

b	index for distribution branches
s	index for damage scenarios
t	index for time instants
U_s	set of branches in service in scenario s
V_s	set of branches out of service in scenario s

Parameters

DI	degradation index
F_s^{Deg}	power flow result in the degradation phase in scenario s
$F_s^{Res}(t)$	power flow result in the restoration phase in scenario s at time instant t
$F_{exp}(t)$	expected MG performance at time instant t
$M(t)$	system performance at time instant t
M_o	pre-event level of system performance
M_{pe}	post-event level of system performance
M_{pr}	post-restoration level of system performance
MRI	microgrid resilience index
$N_{p,b}$	number of poles in branch b
$P_b(t)$	failure probability of branch b at time instant t
$P_{b,l}(t)$, $P_{b,p}(t)$	failure probabilities of branch b at time instant t due to conductor and pole outages, respectively
$P_{p\_ind}(t)$	failure probability of individual poles at time instant t
$P_s(t)$	probability of scenario s at time instant t
REI	restoration efficiency index
VI	vulnerability index
t_e	starting time of the event
t_d	starting time of the degradation phase
t_{pe}	starting time of the post-event status
t_r	starting time of the restoration phase
t_{pr}	starting time of the post-restoration status
t_{ir}	starting time of the infrastructure recovery
t_{pir}	starting time of the post-infrastructure recovery status

and *LOLE* (loss of load expectation) are used to assess the effects of different resilience enhancement measures. Authors in [20] employed Markov chain and MC simulation to account for state transitions of power grids with integrated microgrids (MGs) in extreme events and calculate the indices, respectively. Traditional reliability indices including the loss of load probability (*LOLP*) and the expected demand not supplied (*EDNS*) were modified to describe the power grid survivability in extreme events. A multi-factor grid recovery index and a metric accounting for the expected number of lines on outage were also defined. Operational and infrastructure resilience metrics were introduced and calculated via a MC-based simulation method in [21] to assess the resilience of transmission grids to windstorms.

MGs, due to their inherent features, ensure a higher level of resilience against HILP events as discussed in [4,5,22–26]. A numerical assessment tool is in essence to make a judgment about the MG resilience and plan for further measures to improve it, if necessary. However, there is a gap in the literature for a simple and computationally efficient method capable of quantifying the impact of weather-oriented HILP events on MGs. In case of an approaching event (e.g., a windstorm), it is crucial to quickly get knowledge of possible impacts on the MG so that right decisions are made on proactive preventive measures. Simulation-based techniques are hardly computationally tractable entailing no unique outcome. This paper aims to respond to the need for a simple, computationally efficient, and applicable method for the MG resilience assessment. The proposed analytical method provides a probabilistic model for the degradation impacts of extreme windstorms using fragility curves of components. In contrast to simulation methods widely applied for bulk transmission grids in the literature, the proposed method is simple and computationally efficient with less number of inputs. The change in component failure probabilities (presented by fragility curves) due to temporal effects of the windstorm are accounted for which was neglected in previous works. A suite of numerical metrics is also introduced for quantifying the MG resilience. In contrast to available metrics in the literature, proposed metrics are normalized providing a comparable means for assessing the resilience in various operating conditions and MG systems. In addition, in oppose to traditional reliability indices, proposed metrics are capable of assessing the temporal response of MG against the envisaged windstorm. It is worth noting that the proposed metrics could universally be used for different extreme events. However due to inherent differences in the nature of events and impacts on the power grid, minor revisions should be applied per events (other than windstorms) given the generic framework of this paper. Finally, numerical simulations are conducted and impacts of major factors on MG resilience curve and metrics are investigated through case studies.

2. Quantification of resilience concept

The National Center for Earthquake Engineering Research has offered a general viewpoint on resilience which is applicable to critical infrastructures. This framework consists of 4Rs: robustness, redundancy, resourcefulness, and rapidity [4]. Robustness implies the ability of the system to withstand a specified level of stress or disruption without suffering significant degradation or loss of functionality. Redundancy focuses on the availability of systems, mechanisms, or elements to be activated in order to satisfy functional requirements if significant degradation or loss of functionality occurs. Resourcefulness is the potential to mobilize and apply materials, monetary, informational, technological, and human resources for the sake of diagnosing and solving problems in a prioritized manner. Rapidity is the capacity to restore the system functionality and achieve goals in a timely fashion [27]. In fact, redundancy and resourcefulness are means to achieve the stated goals of resilience, i.e., robustness and rapidity.

As the power system is affected by an extreme event, the system attributes may deteriorate form the normal state. The temporal variation of a system attribute in face of an extreme event is recognized as the system performance. Fig. 1 illustrates a typical curve for the system performance associated with an extreme event considering different MoPs (or system attributes) based on system priorities and objectives [4]. Power system performance can be represented by different MoPs such as the percentage of total or critical loads, number of supplied customers or critical customers, number of survived (or failed) components, and technical metrics such as voltage magnitude or frequency. The operator can prioritize MoPs based on the system operation strategy and objectives. Thus in this paper, the system performance is assessed by supplied load and supplied critical load indices due to high importance and priority of sustainable service delivery to customers of MG.

MG may withstand an extreme event without any significant MoP degradation. The extent of this capability depends on strength level of components provided by hardening measures [8,28], proactive measures taken prior to the event arrival [12,29], and severity of the event. Thus, (t_d–t_e) could be interpreted as a measure of system robustness.

Starting from t_d, the system performance will be downgraded before it settles at M_{pe} when the system enters the post-event state at t_{pe}. At the degradation phase, adaptive operation measures provide the system with some degree of flexibility [30], i.e., lessening the vulnerability level, (M_o–M_{pe}). A vulnerability index (*VI*) is simply introduced to

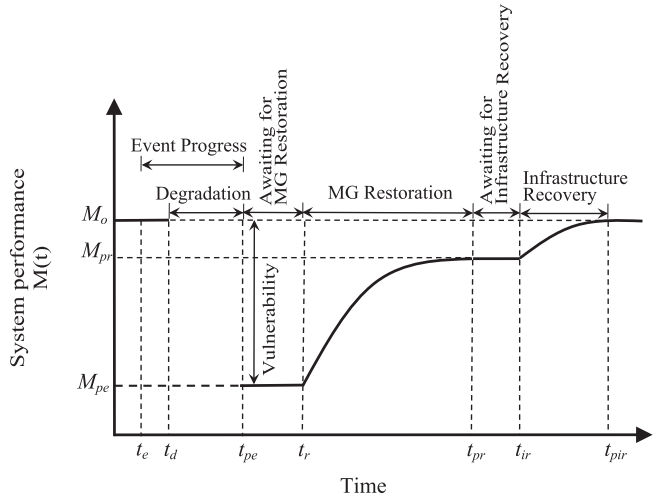

Fig. 1. A typical MoP response associated with an extreme event [4].

evaluate the level of degradation as:

$$VI = \frac{M_o - M_{pe}}{M_o} \tag{1}$$

In which *VI* is 0 in a perfect condition and 1 in a complete degradation. Although *VI* provides a quick perception of how the system performance is impacted by the envisaged event at a glance, it does not convey any information about the temporal behavior of MG. In response to this shortage, a normalized degradation index (*DI*) is proposed as:

$$DI = \frac{\int_{t_d}^{t_{pe}} (M_o - M(t))dt}{M_o(t_{pe} - t_d)} \tag{2}$$

For a fully resistant system, this metric is 0 and *DI* is equal to 1for a weak system with a complete loss of functionality.

From t_{pe} to t_r, the operator gets ready to start the MG restoration. As MG is more agile and its restoration capacity is higher, the duration of preparedness is shorter. Thus, (t_r–t_{pe}) shows how resourceful the MG is against the undesired event.

From t_r, the system enters the restorative phase and recovers quickly to an acceptable level of performance, M_{pr}, at t_{pr}. In this phase, network redundancy (e.g., backup generation and storage, active demand side, etc.) maintains the rapidity of the response. The restoration efficiency index (*REI*) in (3) is a normalized metric to assess the efficiency of restoration phase:

$$REI = \frac{\int_{t_r}^{t_{pr}} (M(t) - M_{pe})dt}{(M_o - M_{pe})(t_{pr} - t_r)} \tag{3}$$

For a MG with a full capacity for restoration, the metric will be 1 and it is 0 for a failed to recover MG.

The MG resilience should be analyzed from the beginning of degradation to the end of restoration. Therefore, (4) represents the MG resilience index (*MRI*) for a specific MoP:

$$MRI = \frac{\int_{t_d}^{t_{pr}} M(t)dt}{M_o(t_{pr} - t_d)} \tag{4}$$

This metric is between 0 and 1 in which higher values correspond with higher MG resilience.

The functionality level of the system in the post-restoration state may not be the same as the initial value before the event, i.e., $M_{pr} \leq M_o$. In fact, the complete restoration of MG is dependent on the infrastructure recovery which may take a longer time, that is, t_{pir} might be much larger than t_{pr}. Infrastructure recovery is dependent on the severity of the event and the crew availability [31]. Starting from the post-restoration time t_{pr} the infrastructure will be in the recovery mode. Similar metrics can be defined to assess the infrastructure recovery phase. This phase, however, is out of the scope of this paper while further discussions are specifically presented in the literature [4].

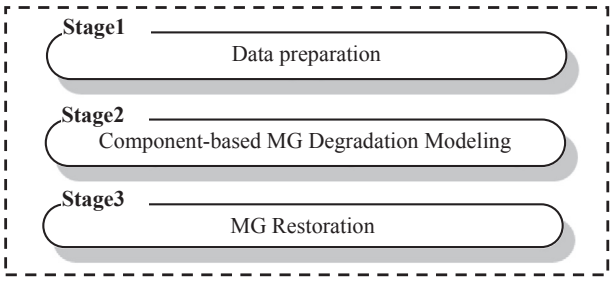

Fig. 2. General scheme for the resilience assessment framework.

3. Resilience assessment framework

The proposed framework depicted in Fig. 2 aims to quantify the MG resilience metrics under an extreme windstorm. Fig. 2 consists of three main stages: data preparation, component-based MG degradation modeling, and MG restoration. The resilience curve and metrics defined in (1)-(4) will be obtained by fulfilling stages 1–3 for a given MoP (particularly supplied load in this work).

3.1. First stage: Data entry

This stage is the input module of the proposed framework. Network-related information, wind-induced fragility curves of components, and predicted event profile are three categories of data imported in this stage. Network data mainly include single line diagram, load characteristics, and information on generation and storage units. Such data provide a picture of the network prior to the major disturbance. Past experiences of windstorms and component fragility curves indicate that distribution poles and conductors and wind-based units are vulnerable entities to windstorms. Wind-based units are tripped at the event due to safety reasons as the wind velocity reaches the cut-out speed of the turbine. Wind-oriented fragility curves of poles and conductors are imported in this stage as model inputs and will be used in the next stage to obtain the system degradation model. These curves show the component outage probability versus the wind speed. Regarding the event data, it is assumed that the upcoming windstorm profile is given by the weather agency. This prediction may either be an estimation of the weather state via satellite information and/or mathematic tools or a real-time recorded profile of the windstorm just experienced in adjacent weather stations (located in the trajectory of the approaching windstorm).

3.2. Second stage: Component-based MG degradation model

This stage is vital for estimating the MG behavior at the degradation phase. The proposed algorithm is illustrated in Fig. 3. The algorithm is a component-based procedure in which fragility curves and the event model are convolved to achieve the degradation of components through which the MG degradation model can be drawn.

3.2.1. Step 1: Estimating fragility of overhead branches

Fragility curves are derived empirically, experimentally, analytically, or through a combination of these methods using expert judgments [32]. Fragility curves of individual poles and conductors are imported in the model and no effort is done to develop these curves in this paper.

The outage probabilities presented in the fragility curves were

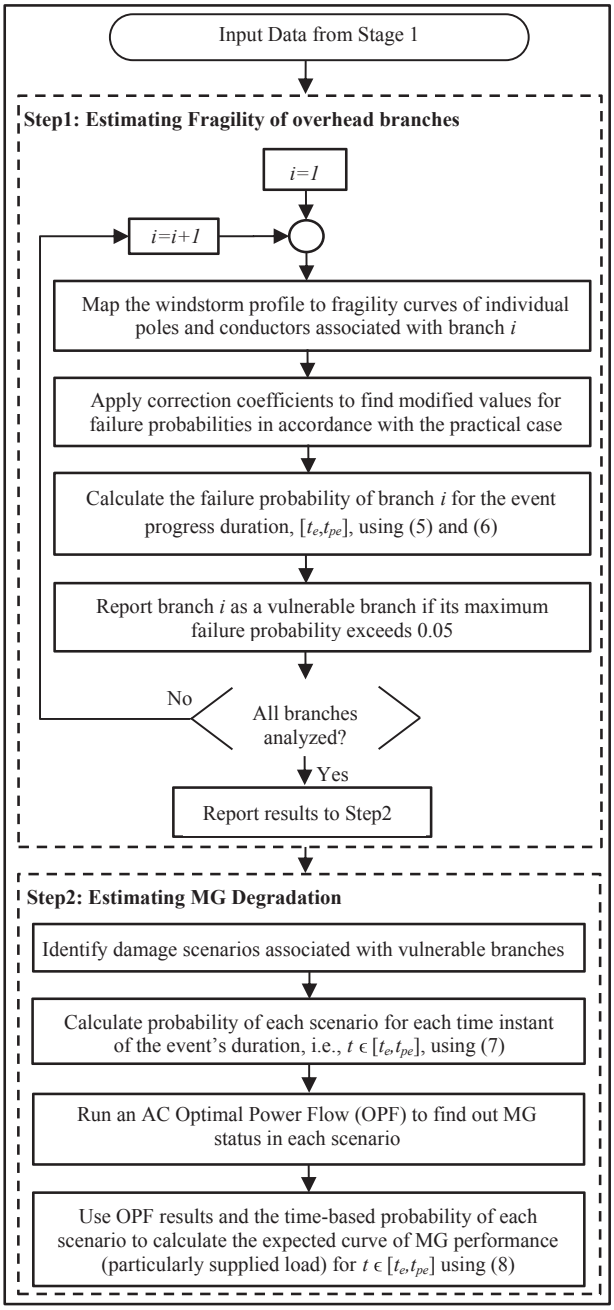

Fig. 3. Flowchart of the component-based MG degradation modeling.

achieved by exposing components to a specified level of stress for a standard duration [32]. These probability values should thus be adjusted for resilience studies when the same component is exposed to a continuous profile of the windstorm [32]. Accordingly, the time-based windstorm profile is mapped into fragility curves of individual poles and conductors to obtain the time-based failure probability of each component. Then, correction (adjusting) coefficients are applied to failure probabilities [32]. The correction coefficients applied at each time instant reflect the component degradation from the windstorm onset to the previous time instant. Using modified failure probabilities of distribution poles and conductors, a branch failure probability will be calculated for the event progress duration, $[t_e,t_{pe}]$ as [33]:

$$P_b(t) = P_{b,l}(t) + P_{b,p}(t) - P_{b,l}(t)P_{b,p}(t) \quad (5)$$

$$P_{b,p}(t) = 1-(1-P_{p\_ind}(t))^{N_{p,b}} \quad (6)$$

Note that a branch is failed if the distribution line (conductor) or any pole between the associated nodes is failed as expressed in (5). In order to improve the computational efficiency of the model, branches with a maximum failure probability of less than a vulnerability threshold during the event progress (here assumed to be 0.05) are disregarded. Other branches are recognized as vulnerable branches and will be considered in the next step. The aforementioned vulnerability threshold makes a compromise between accuracy and computational efficiency of the solution. Applying a higher threshold results in lower accuracy and enhanced computational efficiency due to less number of branches identified as vulnerable.

3.2.2. Step 2: Estimating MG degradation

This step considers the MG behavior during the degradation phase. It is emphasized that we aim to quantify the MG resilience from the load supply perspective. Therefore, we focus on the operational behavior of MG rather than the detailed control procedures during MG transitions. In case of a holistic resilience assessment, for sure, the transient and dynamic studies are critically in essence and a detailed model of the protection system is also required. It is worth noting that although cascading effects may be a serious threat in looped-operated bulk transmission grids, MGs are much less threatened by cascading outages due to their simple topology and less operational complexity.

In this step, at first, the damage scenarios are identified. A damage scenario is defined by a combination of ON (survived) and OFF (failed) states of each branch. The probability of each scenario is derived using failure probability of branches:

$$P_s(t) = \prod_{b\in V_s} P_b(t) \prod_{b\in U_s} (1-P_b(t)) \quad \forall\ t\in [t_e,\ t_{pe}] \quad (7)$$

Then, an AC Optimal Power Flow (OPF) is used to determine the MG status in each scenario which helps determine if load shedding is required for stabilizing the MG. The AC-OPF formulation is taken from [24], whose details are not stated here due to paper space limitation. The proposed OPF consists of an objective function, conventional equality and inequality load flow constraints [24] in addition to droop-based equations for droop-controlled DERs at steady state [34]. The objective function resembles the priority-based load curtailment procedure by minimizing a weighted function of load curtailment. During extreme events, the MG is routinely isolated from the upstream network until the network operator gives the permission to reconnect to the upstream grid. Thus, an islanded MG is considered in this paper to evaluate the proposed resilience metrics. For each droop-controlled DER, there are two equations driving the relation between droop parameters and steady state output. Droop parameters are constant values which are determined based on DER characteristics [34]. Since MGs are geographically small, windstorms pass through the MG within a few minutes. In this circumstance, the output of renewable resources can be assumed constant within the study horizon and the uncertainty of MG states is negligible. Accordingly, renewable resources are modeled as PQ units in the proposed OPF. Using the scenario-based OPF solution associated with the questioned MoP (supplied load or supplied critical load) in the degradation phase, F_s^{Deg}, and the time-based probability of each scenario, $P_s(t)$, the expected MoP in the degradation phase is achieved as follows:

$$F_{\exp}(t) = \sum_s F_s^{Deg} P_s(t) \quad \forall\ t\in [t_e,\ t_{pe}] \quad (8)$$

It is noted that the computational efficiency of the model in this step is increased as a number of branches with a maximum failure probability that is less than a threshold were disregarded at the previous stage. In addition, the number of overhead branches in a MG is limited as a number of branches are underground cables and not vulnerable to windstorms.

3.3. Third stage: MG restoration

Resilience-oriented service restoration after weather-induced extreme events was specifically studied in a few works in the literature. The main goal of this paper is presenting a resilience assessment (and not enhancement) framework and MG restoration is a module of the proposed framework (see Fig. 2). Thus, different restoration strategies could be implemented within this module based on the recovery techniques and methods used by the operator and we only put a judgment on the process using associated metrics. It could be concluded that adopting the optimal restoration strategy is not the point of concern in this paper. Instead, we aim at implementing a typical MG restoration scheme to fulfill the proposed framework and obtain the resilience curve and metrics. It goes without saying that adopting the optimal restoration strategy within this stage enhances the MG resilience accordingly. This stage is comprised of two steps discussed as follows.

3.3.1. Step 1: Post-event system modeling

The system operator takes some actions after the event onset to identify the post-event system model and start the restoration process. As the event is calmed down and the MG is settled at its minimum performance, the network topology is first updated in each scenario of branch outages. In addition, the post-event statuses of components (in service/out of service), restoration power blocks available at each consecutive time slot, and load restoration priorities are accounted for in this stage. These actions are included in the post-event OPF as new constraints. It is noted that droop control mechanism facilitates the multi-islanded MG operation at the post-event state. The probability of each scenario in the MG restoration phase is not time-based since the major event has passed through. Thus, the probability of each scenario at t_{pe} is used as the constant probability of the scenario under consideration in the restoration phase.

3.3.2. Step 2: Implementing the restoration strategy of MG

The restorative actions will enable the MG to recover load points based on their priorities [7,35,36]. Conventional techniques or smart grid technologies (e.g., self-healing or auto-loop features) could easily be employed in the restoration module regardless of the general procedure of the resilience assessment. Here just for simplification, we take a typical restoration scheme with a predefined restoration process.

In the restoration scheme taken here, demand blocks are recovered in each time slot in a priority-based load restoration process. The restoration resources are demand-side and utility DERs. We assumed that the restoration power is provided in consecutive one-minute time slots. An AC-OPF is run for each scenario to obtain the MG performance from the load supply viewpoint. The AC-OPF is similar to the one taken in the degradation phase and widely used by researchers in the literature [24,34]. It is noted that the infrastructure recovery is not a point of concern in this study and we focus on operational restoration. All operational needs in the restoration process (e.g., adaptive protection and control systems) are assumed to be satisfied while we do not deal with such details. Using the scenario-based restoration results for the questioned MoP obtained in consecutive time steps through the AC-OPF, $F_s^{\mathrm{Res}}(t)$, the expected MoP for the restoration phase is obtained using the probability of each scenario, $P_s(t_{pe})$, as follows:

$$F_{\exp}(t) = \sum_s F_s^{\mathrm{Res}}(t) P_s(t_{pe}), \quad \forall\ t \in [t_{pe}, t_{pr}] \tag{9}$$

4. Numerical simulations

4.1. Case study

In this section, we aim to test the performance of the analytical framework and ensure the sensitivity of the proposed metrics to major influencing factors. We consider the modified IEEE 33-bus distribution test system, shown in Fig. 4, to examine the proposed method. MGs are normally small-scale both from geographic and electric points of view. Compared to the dimensions of real-world MGs, the IEEE 33-bus distribution network is deemed as a large-scale MG. This test system can be operated in the islanded mode by disconnecting at the point of common coupling (PCC) and is widely used by researchers in the literature. The feeder parameters and load data are taken from [37]. The test system consists of residential, commercial, and industrial customers [34]. The proposed case study was implemented in GAMS (to solve the proposed OPF) and MATLAB (to build outage scenarios and quantify proposed metrics) simulation environments. Five dispatchable DER units are included in the test system. The data related to these units are given in Table 1. In addition, two wind turbines (WTs) each with a 0.5 MW rating are installed at buses 16 and 19. It is assumed that prior to the event onset, both wind units are operating at their nominal outputs. Moreover, wind power generation is limited by the cut out speed of 25 m/s [38]. Five photovoltaic (PV)-based DER units each of 0.2 MW rating are installed at buses 5, 7, 13, 21, 27. However, it is assumed that each PV unit produces 0.1 MW based on the solar radiation forecast. Five electric vehicle (EV) parking lots are allocated in the MG as shown in Table 2 [34]. Parking lots are considered as P-Q loads/storage resources in the power flow model.

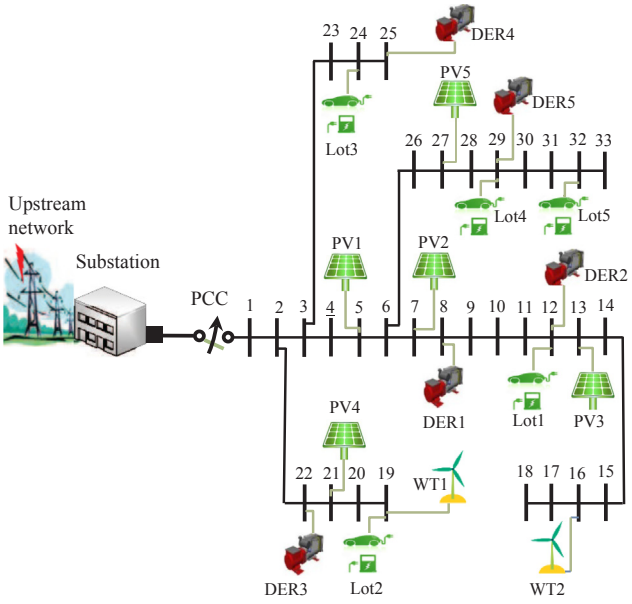

Fig. 4. Modified IEEE 33-bus electric distribution test system.

Also, 70% of EVs are plug-in hybrid EVs (PHEVs) with a battery capacity of 7.2 kWh and the remaining EVs are plug-in EVs (PEVs) with a battery capacity of 23 kWh. In addition, the lower bound of EV charging/discharging is 1.1 kW and the upper bounds are 2.2 and 3.8 kW for PHEVs and PEVs, respectively [38]. It is arbitrarily assumed that, in overall, 42% of the EVs in the parking lot were already scheduled to be charged with their maximum power rate at the study time. Considering the base demand, 3.715 MW [37], and the EV load, the total MG demand at the study time horizon is 4 MW which is chosen

Table 1
DER locations, ratings, and operating modes.

DER#	Bus#	$\overline{P}_i^G$ (MW)	$\underline{P}_i^G$ (MW)	$\overline{Q}_i^G$ (MVAR)	$\underline{Q}_i^G$ (MVAR)	Mode
DER1	8	1	0.10	0.80	−0.80	Droop
DER2	12	0.40	0.04	0.30	−0.30	Droop
DER3	22	0.40	0.04	0.30	−0.30	Droop
DER4	25	0.40	0.04	0.30	−0.30	Droop
DER5	29	1	0.10	0.80	−0.80	Droop

Table 2
Parameters of allocated parking lots [34].

Lot #	Bus #	Lot Capacity (# of EVs)	Lot EVs/Lot Capacity (%)	Type
1	12	60	100	Residential
2	19	100	40	Residential
3	24	60	40	Commercial
4	29	60	40	Commercial
5	32	100	100	Residential

as the base power (S_{base} = 4 MVA). The upper and lower node voltage limits are 1.05 and 0.95 p.u., respectively. A maximum steady-state frequency variation of ± 0.005 p.u. is considered in case studies [34].

The proposed method is tested under an approaching windstorm. Since the MG is geographically small, a single weather forecast site is assumed for the whole MG. The event profile is taken from a recorded windstorm just experienced in an adjacent weather station and roughly used as the estimation of the approaching windstorm profile in MG. It may take a windstorm several hours to pass through bulk transmission grids. However, a windstorm on its trajectory may pass through a MG quickly (i.e., within several minutes) affecting all components at the same time [30].

Distribution branches 2-3, 5-6, 10-11, 21-22, 24-25 and 31-32 are vulnerable to the extreme event. We assume the remaining distribution branches are underground cables or overhead branches which reinforced highly against windstorms. The restoration time is 15 min in all case studies and the resilience metrics are calculated associated with this time horizon.

All simulations were executed on a PC with Intel Core i7 CPU @ 3.20 GHz and 4 GB RAM. The computation time in the case study under consideration was 320 *s* which further illustrates the applicability of the proposed method for assessing the MG resilience to an approaching windstorm. The execution of the proposed method on the IEEE 33-bus distribution network is not computationally cumbersome; thus, its application on larger sizes (if any in MGs' world) would not be problematic.

4.2. Numerical results

The occurring windstorm profile is depicted in Fig. 5. Four cases are defined and analyzed as follows in which we consider Pattern I in Cases 0-II and apply by Pattern II in Case III.

4.2.1. Case 0: Base case

In this case, Fig. 6 depicts a normal fragility curve for overhead distribution branches. The restoration process is based on a distributed capacity of 1000 kW which is available from the aggregation of small generation and storage blocks provided jointly by the utility and demand side at different nodes across the MG. This restored capacity in Fig. 7 is ascending with time due to the gradual utilization of distribution generation for the demand side restoration.

Fig. 7 depicts the resilience curve in terms of the MG supplied loads. According to our assumptions, wind units stop operating at wind speeds higher than 25 m/s. This capacity loss would be the cause of the first significant degradation in the resilience representative curve. In Fig. 7, the MG performance is degraded suddenly by 0.12 p.u. (or 12%) at t = 1.25 min. This degradation takes place prior to the degradation due to the outages of overhead branches, which will be initiated afterward. The wind energy degradation could be inferred that the MG robustness in our example is influenced significantly by the loss of wind turbines in windstorms. Thus, a higher penetration of wind power could be interpreted as less robustness to windstorms in this MG.

From this point onward in Fig. 7, the resilience curve experiences the degradation due to the outages of overhead distribution branches. This degradation is represented by a sharp decline of 0.25 p.u. from 0.87 to 0.63 p.u. at t = 3.2 min. The MG performance degradation depends on the extreme event severity, the MG operating point prior to the extreme event, and the MG response to the extreme condition as it unfolds. In Fig. 7, the MG will be subjected to a smaller degradation slope if it is characterized by sufficient counteractive measures and mechanisms to handle extreme conditions. Over time, the restoration process has compensated about 32.5% of the lost load in MG as shown in Fig. 7. The additional restoration of MG load would require participation by the ground crew and a significant infrastructure recovery which may take longer.

4.2.2. Case I

In this case to demonstrate the impact of distributed generation on the restoration process and the resilience curve, a concentrated capacity of 1000 kW via a droop-controlled backup generating unit located at bus 14 is assumed to be available in place of that in Case 0 for the restoration process. Other assumptions stated in Case 0 will hold. Fig. 8 illustrates the resilience curves in terms of the MG supplied loads in Cases 0 and I. As expected, only the restorative phase, when we intend to retrieve the lost load, will be affected by the variation of the available generation capacity. The restoration process has only compensated about 5.5% of the lost load in Case I while a 32.5% of the lost load was accounted for in Case 0. That is, the restoration process in Case 0 was more effective than that in Case I. The reason is that the available generation capacity for restoration in Case 0 was distributed as small blocks in several buses while in Case I the generation capacity is concentrated at bus 14, which to some extent could be more difficult to utilize as the MG restoration process entails the availability of the distribution grid for the utilization of the accessible generation capacity.

4.2.3. Case II

To investigate the impact of system reinforcement on the resilience curve, we consider the reinforced (hardened) fragility curves depicted in Fig. 6. Accordingly, the forced outage rates of distribution system branches in Case II are much lower than those in Case 0. Other assumptions stated in Case 0 still hold. Fig. 9 shows the resilience curves in terms of the MG supplied loads in Cases 0 and II. The impact of system reinforcement appears in the degradation phase. Since the extreme event patterns in Cases 0 and II are the same, the MG downgrade due to the loss of wind turbines stated in Case 0 applies to Case II as well. However, the degradation of MG performance due to the outages of overhead distribution branches in Case II is significantly lower than that in Case 0. In Fig. 9, the post-degradation system performance in Case II is significantly superior to that in Case 0. Furthermore, the post-restoration system performance in Case II is higher than that in Case 0. It can be inferred that the MG in Case II, when the overhead distribution branches are reinforced against windstorms, is slightly degraded during the extreme event and almost completely recovered during the restoration process.

4.2.4. Case III

We apply the Pattern II shown in Fig. 5 to study the impact of

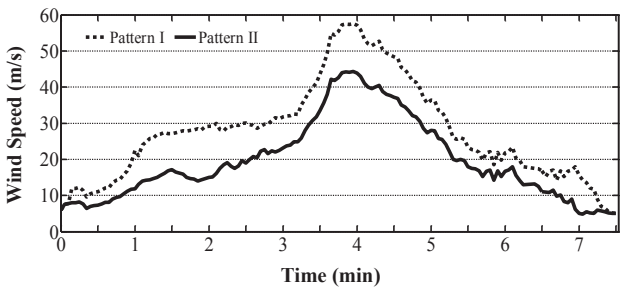

Fig. 5. Forecasted profile for the approaching windstorm.

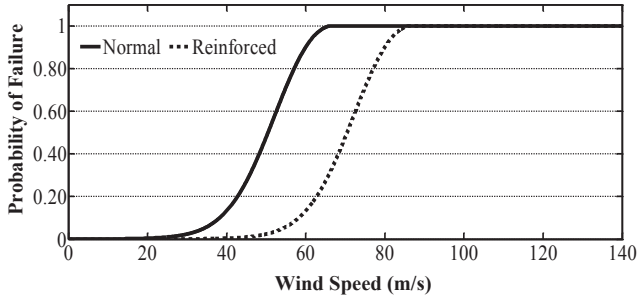

Fig. 6. A typical fragility curve for distribution branches.

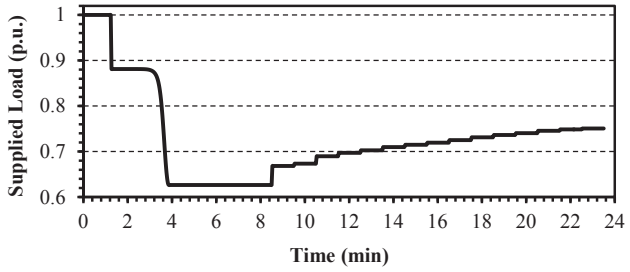

Fig. 7. Resilience curve in case 0.

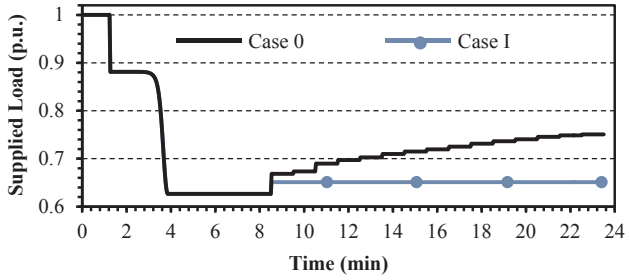

Fig. 8. Resilience curves in Cases 0 and I.

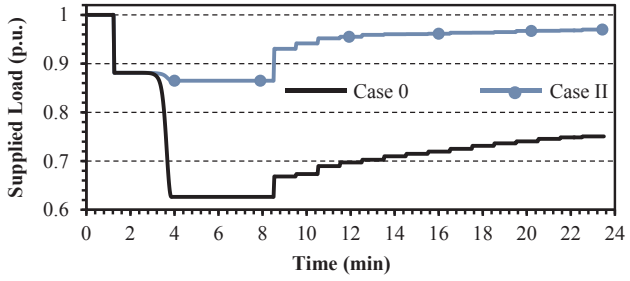

Fig. 9. Resilience curves in Cases 0 and II.

extreme event severity on the resilience curve. Other assumptions stated in Case 0 still hold. Fig. 10 presents the resilience curves in terms of the MG supplied loads in Cases 0 and III. According to Fig. 5, the primary source of the MG downgrade, which is the sudden loss of wind turbines, is experienced a bit later in Case III. In essence, the MG downgrade occurs at $t = 3.2$ min in Case III while it occurs at $t = 1.25$ min in Case 0 (see Figs. 5 and 10). In Case III, the probability of branch outages in power distribution system is lower than those in Case 0. Thus, the degradation of MG performance due to such outages in Case III is significantly less than that of Case 0. The post-degradation system performance in Case III is also significantly better than that of Case 0. Thus, the post-restoration system performance in Case III is better than that in Case 0.

4.3. Case comparisons

Table 3 presents the proposed resilience metrics calculated based on the resilience curves associated with case studies. Since the critical load supply is important in the power system resilience assessment, the proposed metrics are calculated for both supplies of total and critical loads as MoPs. Considering *VI* and *DI* metrics, we observe a lowering characteristic in each MoP. As discussed earlier for resilience curves, the degradation will be lower if overhead distribution branches are reinforced or the extreme event is less severe. This point is demonstrated in Table 3 by comparing *VI* and *DI* values in Cases II and III with those in Cases 0 and I for both MoPs. In addition, the MoP for critical loads does not experience a significant degradation due to the priority-based mechanism adopted for load shedding. Considering the MoP in terms of total loads in Cases 0 and I, we encounter a 27.87% degradation in *DI* although *VI* shows a 37.35% vulnerability. The resilience focuses on both degradation value and time. Therefore, *DI* is more meaningful than *VI* in the resilience assessment and enhancement studies. The same discussion applies to distinguishing *VI* and *DI* in Cases II and III in terms of supplying total loads and all cases pertaining to critical loads.

In Table 3, *REI* describes the restoration efficiency whose values depend not only on the restoration process but also on the outage probability of distribution branches, dominant outage scenario and the restoration starting point. *MRI* offers normalized values which facilitate the comparison of resilience features in different case studies or different MG systems. For both supplied total and critical load MoPs, the largest *MRI* is obtained in Case II where the MG system reinforcement is taken into account.

4.4. Discussions

Cases I and II (defined in section IV.B) investigated the impact of restoration strategy (as an operational factor) and component strength (as a hardening factor) on MG resilience. Although these case studies give a primary interpretation of main influencing factors, they are not sufficient to make optimal decisions on resilience enhancement measures. In addition, uncoordinated resilience enhancement measures may result in undesired consequences. For instance, replacing overhead branches with underground routs increases the MG resilience to windstorms while the MG resilience is decreased against floods. Thus, in contrast to reliability metrics which generally report the system behavior to a set of events, resilience metrics should be attributed to a specific hazard. To ensure the optimality of resilience improvement decisions, the impact of a resilience enhancement measure should separately be assessed against a set of possible weather events by means of the proposed framework. A compromise should then be made on effects of the resilience enhancement measure against different hazards. We do not, however, deal with resilience enhancement measures and only provide an assessment framework to evaluate their impacts.

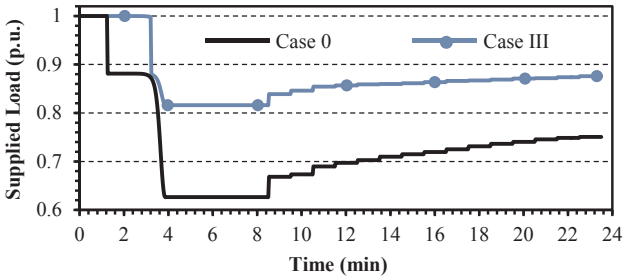

Fig. 10. Resilience curves in Cases 0 and III.

Table 3
Comparative results for MG resilience metrics.

MoP	Case Study	Index (Metric)			
		VI	*DI*	*REI*	*MRI*
Total Load	0	0.3735	0.2787	0.2420	0.7141
	I	0.3735	0.2787	0.0655	0.6696
	II	0.1351	0.1290	0.6962	0.9300
	III	0.1839	0.1776	0.2512	0.8516
Critical Load	0	0.1218	0.0964	0.2376	0.9048
	I	0.1218	0.0964	0.0010	0.8854
	II	0.0577	0.0559	0.0091	0.9431
	III	0.0717	0.0698	0.0028	0.9288

5. Conclusion

This paper presented a quantitative framework for the MG resilience assessment against weather-oriented events using the concept of component fragility curves. Although the framework was mainly tailored for windstorms in this work, it can easily be modified for other events. The proposed method establishes a probabilistic component-based MG degradation framework by jointly employing fragility curves of components and windstorm model. The proposed analytic method is simple and computationally efficient providing a helpful means for MG resilience assessment in the extreme condition of an approaching windstorm. Proposed metrics are normalized which offers a comparable tool for assessing the resilience in various operating conditions and power systems. The efficiency and the essence of the proposed framework in response to an approaching windstorm, were tested on a 33-bus droop-controlled MG. The numerical results showed that the proposed method is able to quantitatively display the MG behavior in response to the extreme windstorm. Without the loss of generality, the supplied load quantity was chosen as the MoP in this paper. The sensitivity of resilience curves and metrics to influencing factors was investigated by using comparative studies. The proposed framework can be used as a numerical assessment tool by responsible parties for making decisions on resilience enhancement measures (particularly against windstorms). Future work will present further investigations to recognize the feasibility of remedial measures for enhancing the power system resilience.

Acknowledgement

This work was supported by the Iran National Science Foundation (INSF) under grant No. 95834085.

References

[1] Panteli M, Mancarella P. The grid: stronger, bigger, smarter?: presenting a conceptual framework of power system resilience. IEEE Power Energ Mag 2015;13(3):58–66.
[2] Chang L, Wu Z. Performance and reliability of electrical power grids under cascading failures. Int J Electr Power Energy Syst 2011;33(8):1410–9.
[3] Amirioun MH, Aminifar F, Lesani H. Resilience-oriented proactive management of microgrids against windstorms. IEEE Trans Smart Grid 2018;33(4):4275–84.
[4] Li Z, Shahidehpour M, Aminifar F, Alabdulwahab A, Al-Turki Y. Networked microgrids for enhancing the power system resilience. Proc IEEE 2017;105(7):1289–310.
[5] Chanda S, Srivastava AK. Defining and enabling resiliency of electric distribution systems with multiple microgrids. IEEE Trans Smart Grid 2016;7(6):2859–68.
[6] Gholami A, Aminifar F, Shahidehpour M. Front lines against the darkness: enhancing the resilience of the electricity grid through microgrid facilities. IEEE Electrif Mag 2016;4(1):18–24.
[7] Gao H, Chen Y, Xu Y, Liu C-C. Resilience-oriented critical load restoration using microgrids in distribution systems. IEEE Trans Smart Grid 2016;7(6):2837–48.
[8] Manshadi SD, Khodayar ME. Resilient operation of multiple energy carrier microgrids. IEEE Trans Smart Grid 2015;6(5):2283–92.
[9] Chen J, Thorp JS, Dobson I. Cascading dynamics and mitigation assessment in power system disturbances via a hidden failure model. Int J Electr Power Energy Syst 2005;27(4):318–26.
[10] Shi B, Liu J. Decentralized control and fair load-shedding compensations to prevent cascading failures in a smart grid. Int J Electr Power Energy Syst 2015;67:582–90.
[11] Bompard E, Huang T, Wu Y, Cremenescu M. Classification and trend analysis of threats origins to the security of power systems. Int J Electr Power Energy Syst 2013;50:50–64.
[12] Amirioun MH, Aminifar F, Lesani H. Towards proactive scheduling of microgrids against extreme floods. IEEE Trans Smart Grid 2018;9(4):3900–2.
[13] Gholami A, Shekari T, Amirioun MH, Aminifar F, Amini H, Sargolzaei A. Toward a consensus on the definition and taxonomy of power system resilience. IEEE Access 2018;6:32035–53.
[14] Panteli M, Mancarella P. Influence of extreme weather and climate change on the resilience of power systems: impacts and possible mitigation strategies. Electr Power Syst Res 2015;127:259–70.
[15] Khodaei A, et al. Guest editorial power grid resilience. IEEE Trans Smart Grid 2016;7(6):2805–6.
[16] Wang Y, Chen C, Wang J, Baldick R. Research on resilience of power systems under natural disasters—a review. IEEE Trans Power Syst 2016;31(2):1604–13.
[17] Panteli M, Trakas DN, Mancarella P, Hatziargyriou ND. Power systems resilience assessment: hardening and smart operational enhancement strategies. Proc IEEE 2017;105(7):1202–13.
[18] Ma C, Xiao X, Li C, Zhang Y, Li H. Uncertain risk assessment model for catastrophic accidents in power system. Int J Electr Power Energy Syst 2014;62:374–82.
[19] Panteli M, Mancarella P. Modeling and evaluating the resilience of critical electrical power infrastructure to extreme weather events. IEEE Syst J 2017;11(3):1733–42.
[20] Liu X, Shahidehpour M, Li Z, Liu X, Cao Y, Bie Z. Microgrids for enhancing the power grid resilience in extreme conditions. IEEE Trans Smart Grid 2017;8(2):589–97.
[21] Panteli M, Mancarella P, Trakas D, Kyriakides E, Hatziargyriou N. Metrics and quantification of operational and infrastructure resilience in power systems. IEEE Trans Power Syst 2017;32(6):4732–42.
[22] Farzin H, Fotuhi-Firuzabad M, Moeini M. Enhancing power system resilience through hierarchical outage management in multi-microgrids. IEEE Trans Smart Grid 2016;7(6):2869–79.
[23] Gholami A, Shekari T, Grijalva S, Proactive management of microgrids for resiliency enhancement: an adaptive robust approach, IEEE Trans Sustain Energy, to be published.
[24] Gholami A, Shekari T, Aminifar F, Shahidehpour M. Microgrid scheduling with uncertainty: the quest for resilience. IEEE Trans Smart Grid 2016;7(6):2849–58.
[25] Chen C, Wang J, Qiu F, Zhao D. Resilient distribution system by microgrids formation after natural disasters. IEEE Trans Smart Grid 2016;7(2):958–66.
[26] Xu Y, Liu C-C, Schneider K, Tuffner F, Ton D. Microgrids for service restoration to critical load in a resilient distribution system. IEEE Trans Smart Grid 2018;9(1):426–37.
[27] Bruneau M, et al. A framework to quantitatively assess and enhance the seismic resilience of communities. Earthq Spectra 2003;19(4):733–52.
[28] Ma S, Chen B, Wang Z. Resilience enhancement strategy for distribution systems under extreme weather events. IEEE Trans Smart Grid 2018;9(2):1442–51.
[29] Mohagheghi S, Rebennack S. Optimal resilient power grid operation during the course of a progressing wildfire. Int J Electr Power Energy Syst 2015;73:843–52.
[30] Wang C, Hou Y, Qiu F, Lei S, Liu K. Resilience enhancement with sequentially proactive operation strategies. IEEE Trans Power Syst 2017;32(4):2847–57.
[31] Arab A, Khodaei A, Han Z, Khator SK. Proactive recovery of electric power assets for resiliency enhancement. IEEE Access 2015;3:99–109.
[32] Shafieezadeh A, Onyewuchi UP, Begovic MM, DesRoches R. Age-dependent fragility models of utility wood poles in power distribution networks against extreme wind hazards. IEEE Trans Power Deliv 2014;29(1):131–9.
[33] Panteli M, Trakas DN, Mancarella P, Hatziargyriou ND. Boosting the power grid resilience to extreme weather events using defensive islanding. IEEE Trans Smart Grid 2016;7(6):2913–22.
[34] Abdelaziz MMA, Shaaban MF, Farag HE, El-Saadany EF. A multistage centralized control scheme for islanded microgrids with PEVs. IEEE Trans Sustain Energy 2014;5(3):927–37.
[35] Chen C, Wang J, Ton D. Modernizing distribution system restoration to achieve grid resiliency against extreme weather events: an integrated solution. Proc IEEE 2017;105(7):1267–88.
[36] Lei S, Wang J, Chen C, Hou Y. Mobile emergency generator pre-positioning and real-time allocation for resilient response to natural disasters. IEEE Trans Smart Grid 2018;9(3):2030–41.
[37] Baran ME, Wu FF. Network reconfiguration in distribution systems for loss reduction and load balancing. IEEE Trans Power Deliv 1989;4(2):1401–7.
[38] Amirioun MH, Kazemi A. A new model based on optimal scheduling of combined energy exchange modes for aggregation of electric vehicles in a residential complex. Energy 2014;69:186–98.